University of Bath

Alternative formats
If you require this document in an alternative format, please contact:
openaccess@bath.ac.uk

ARTICLE

Effect of mono- and divalent extra-framework cations on the structure and accessibility of porosity in chabazite zeolites

Huan V. Doan,[*a,b] Ka Ming Leung,[c] Valeska P. Ting[*d] and Asel Sartbaeva[*e]

Chabazite (CHA), one of the most common zeolite framework types, has a remarkable capacity to accommodate a wide range of different cations within the unique CHA framework. This has led to CHA being applied extensively in ion exchange, and studied for highly selective gas sorption, most notably through a trapdoor mechanism. Here, we report the systematic study of a series of six chabazite zeolites (*i.e.* K-CHA, Cs-CHA, Ca-CHA, Ba-CHA, Sr-CHA and Zn-CHA) obtained by subjecting the parent chabazite (KNaCHA) to exchange operations with cations of different valences and atomic radii. These samples were examined using numerous techniques and it was found that the differences in valence and size between extra-framework cations exert a significant effect on the abundance of these cations positioned in the framework, resulting in differing nitrogen sorption ability measured in the synthesised chabazite zeolites. These findings will help to understand how the zeolite counter-cation affects the ability of the CHA material to selectively sequester and separate gases through the use of the trapdoor mechanism.

1. Introduction

Zeolites, as an industrially-relevant class of porous crystalline materials, have attracted significant attention because of their exchangeable extra-framework cation sites[1–3] and their versatility in various applications such as gas separation and storage,[4–9] gas sensors[10–13] and catalysis.[14–17] Zeolites consist of an aluminosilicate framework, made of almost rigid SiO_4 and AlO_4 tetrahedra connected through oxygen atoms. There are about 250 different types of synthesisable, unique zeolites recognised by the International Zeolite Association (IZA).[18] These are given a three-letter code, which identifies each framework. Some of the most commonly studied zeolites are made of following frameworks: MFI,[19–22] FAU,[23–25] LTA,[26–29] CHA[30–35] and EMT.[36–39] Because zeolites have found so many uses, there has been a considerable push to predict which zeolites could be synthesised,[40,41] how new zeolites could be produced,[36,42,43] and what new properties could be designed and developed among known zeolites. Post-synthetic modification for developing new forms of existing zeolites is a simple approach, which has also been seen in the related area of study of metal-organic frameworks.[44,45]

Chabazite zeolites (CHA) which were heavily studied in the past have attracted the attention of the zeolite community because

a. School of Chemistry, University of Bristol, Bristol BS8 1TS, UK.
b. Department of Oil Refining and Petrochemistry, Hanoi University of Mining and Geology, Duc Thang, Bac Tu Liem, Hanoi, Vietnam.
c. Department of Chemistry, The University of Hong Kong, Pokfulam, Hong Kong SAR, China.
d. Department of Mechanical Engineering, University of Bristol, Bristol BS8 1TR, UK.
e. Department of Chemistry, University of Bath, Bath BA2 7AY, UK.
*Authors for correspondence: huan.doan@bristol.ac.uk (HVD), v.ting@bristol.ac.uk (VPT) and a.sartbaeva@bath.ac.uk (AS)
Electronic Supplementary Information (ESI) available: [details of any supplementary information available should be included here]. See DOI: 10.1039/x0xx00000x

of their usefulness for a wide variety of applications. As mentioned previously, these chabazite zeolites have been widely reported as being efficient catalysts for chemical processes such as the conversion of methanol to olefins[46,47] and selective catalytic reduction of NO_x.[48,49] The charge difference between the Si and Al atoms in CHA is balanced by extra-framework cations ("counter cations") that are loosely bound to the negatively charged chabazite framework. Recently, CHA materials having Cs^+ and K^+ as their counter cations have been shown to have significant potential in highly discriminative gas separations as a result of the extra-framework cations acting as selective trapdoors.[50] Their ability to preferentially adsorb CO_2 over N_2 has led to these zeolites being tested for CO_2 capture and sequestration.[51,52] However, these studies did not systematically address the role of the counter cation in the highly selective trapdoor mechanism. Understanding the role of the extra-framework cations in this selective adsorption is important for the design of further materials that can be applied to selective separations.

As noted previously, the gas sorption ability mainly depends on the properties of the counter-cations in these chabazite zeolites.[53–58] For example, in chabazite zeolites with an Si/Al ratio of ~2, the samples with cations such as K^+, Cs^+ and Li^+ adsorb nitrogen to a far lesser extent than those with cations such as Ca^{2+}, Ba^{2+} and Mg^{2+}.[53] This could be attributed to a range of possible factors. Site preference could be used to explain this difference because most of the monovalent cations which have been reported so far favour a position in the centre of the eight-membered ring (8MR)[55] which is supposedly the most accessible window for adsorption of gases (see Figure 1a and b for the three different rings available within a CHA framework). In addition, the size of cations also plays an important role in the gas adsorption capacity of chabazite (see Figure 1c).[59] Larger

ions lead to a higher energy barrier ΔE for guest molecules because they have a stronger interaction with the local environment of the 8MR. For example, the nitrogen BET surface area of Cs-CHA (with ΔE = 508 meV) is higher than that of K-CHA which has ΔE = 278 meV.[54] The density of cations is also important for the adsorption ability of chabazite. A higher density of cations could lead to a higher energy barrier ΔE because of the electrostatic repulsive interactions of cations in chabazite.
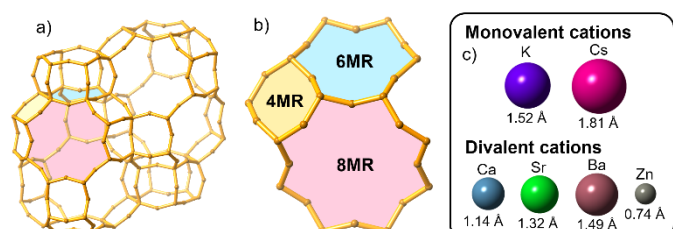

Figure 1. Different characteristics of the CHA framework: a) CHA framework; b) Three different ring windows in chabazite; c) Possible extra-framework cations in chabazite, showing indicative atomic sizes.[60] Images generated using CrystalMaker®: a crystal and molecular structures program for Windows. CrystalMaker Software Ltd, Oxford, England.

Shang et al.[53,54,61] and Ridha et al.[55] have published extensively on size and position of extra-framework cations in various chabazite zeolites such as Li-CHA, K-CHA, Cs-CHA and Ca-CHA, yet none of the previous studies so far have drawn a direct comparison between monovalent and divalent cations in these materials. Since some chabazite zeolites such as Ca-CHA showed significantly higher surface areas than K-CHA (649 m^2 g^{-1} compared to 20 m^2 g^{-1}, from N_2 Langmuir surface area measurements),[61] the valence difference between the extra-framework cations might be an important factor in the estimation of the gas sorption capacity/separation ability in chabazite.

This research aimed to produce a series of chabazite zeolites (K-CHA, Cs-CHA, Ca-CHA, Ba-CHA, Sr-CHA and Zn-CHA) to compare the structures of those zeolites with a view to determining if the monovalent and divalent cations would affect the gas separation properties. These chabazite zeolites were characterised by a range of techniques to understand the correlation between the nature of extra-framework cations, the structure of CHA framework after ion exchange and the accessibility of the internal surface area available for gas separation and sequestration.

2. Experimental

2.1. Synthesis of chabazite

The raw material used for the chabazite synthesis was zeolite Y (334413-100G, Aldrich) with a composition of 0.17 Na_2O : Al_2O_3 : 8 SiO_2 : 500 H_2O. First of all, 5 g of zeolite Y was dehydrated in an oven under vacuum at 450 ^oC for 6 h, with a heating rate of 2 ^oC min^{-1}. Then ~4 g of this zeolite Y was added to the mixture of 31.6 ml distilled water and 4.3 ml KOH 45%, stirring for 30 s and then heated in an oven at 95 ^oC for 96 h. After that, the product was washed with 500 ml distilled water then dried at room temperature to obtain a parent chabazite sample (KNa-

CHA), as confirmed via powder X-ray diffraction analysis. Hereafter, this sample will be referred as the parent zeolite.

2.2. Ion exchange of chabazite

2 g of parent chabazite was ion-exchanged with either 80 ml of 1M KCl (Fisher, 99%), 80 ml of 1M CsCl (Fisher, 99%), 40 ml of 1M $CaCl_2$ (Fisher, 99%), 40 ml of 1M $SrCl_2$ (Fisher, 99%), 40 ml of 1M $BaCl_2$ (Fisher, 99%) or 40 ml of 1M $ZnCl_2$ (Fisher, 99%) at 70 ^oC, stirring continuously at 300 rpm for 24 h to produce the ion-exchanged CHA zeolites. The products then were washed with distilled water until a supernatant with pH 7 was achieved. These ion-exchanged chabazite zeolites were named K-CHA, Cs-CHA, Ca-CHA, Sr-CHA, Ba-CHA and Zn-CHA, respectively.

The synthesised samples were characterised by powder X-ray diffraction (PXRD), scanning electron microscopy (SEM), energy-dispersive X-ray spectroscopy (EDX), solid-state magic angle spinning nuclear magnetic resonance (SS MAS NMR) and gas sorption analysis. The details of these experiments are included in the Supplementary data.

3. Results and discussion

Phase purity and crystallinities of the synthesised chabazite sample and ion-exchanged samples were confirmed by powder X-ray diffraction. Firstly, Figure 2a shows PXRD patterns for commercial zeolite Y, heated zeolite Y, synthesised parent chabazite zeolite and simulated chabazite zeolite. After the heat treatment, it can be seen that zeolite Y retains the same crystallinity as the commercial sample with no changes in the framework structure. As expected, we only observe some slight broadening of higher 2θ peaks. However, after crystallisation, significant differences can be observed in the PXRD pattern; i.e. a high-intensity peak at 6 degrees 2θ in zeolite Y disappears, higher peaks are seen at 11 and 21 degrees 2θ, as well as a considerably more intense peak at 33 degrees 2θ. The PXRD pattern of the parent chabazite zeolite was compared with the simulated CHA framework zeolite prepared by Calligaris et al.[62] Every peak in the PXRD pattern of simulated chabazite zeolite is seen in that of parent chabazite zeolite with a similar intensity, demonstrating that the CHA framework was formed in the synthesised sample.
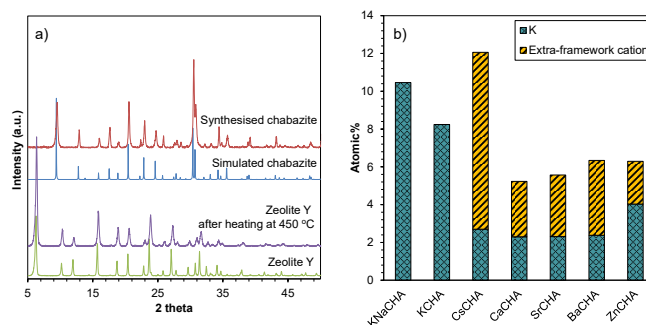

Figure 2. a) PXRD patterns of commercial zeolite Y (before and after heat treatment at 450 ^oC) and chabazite zeolites (simulated and synthesised). PXRD spectra are offset in intensity, for clarity. b) The proportion of extra-framework cations compared to potassium in chabazite zeolites, produced from EDX results as detailed in Table S3 in the SI.

After successful phase identification, both Le Bail and Rietveld analyses were attempted on parent and exchanged zeolite PXRD data. While the data was not of sufficient quality to allow detailed Rietveld analysis, the results of the Le Bail refinement showed the average unit cell dimensions of the CHA materials containing divalent counter cations were consistently smaller than those containing monovalent cations (e.g. average of a = 9.462(1)Å for monovalent and average a = 9.442(7)Å for the divalent cations, with the range in the last decimal place in brackets). The extracted Le Bail unit cell parameters are included in Supplementary data (Table S2).

Secondly, after ion exchange, all chabazite zeolites were studied using energy-dispersive X-ray spectroscopy to estimate the elemental composition in each sample. From the EDX data shown in Figure S3 and Table S3 in Supplementary data, there is very little Na^+ remaining in the parent KNa-CHA zeolite. This suggests that Na^+ was almost completely exchanged by K^+ during synthesis. Thus, it was assumed that the structure and properties of K-CHA and KNa-CHA would be similar. The EDX data indicate that the ratio of Si/Al in the chabazite zeolites is close to 2 in all ion-exchanged chabazite and parent chabazite. The proportion of extra-framework cations compared to potassium in each chabazite is exhibited in Figure 2b, showing that Cs^+, Ca^{2+}, Ba^{2+}, Sr^{2+} and Zn^{2+} have been taken up successfully in the material by ion-exchange method. However, a proportion of residual potassium is still present in Cs-CHA, Ca-CHA, Ba-CHA, Sr-CHA and Zn-CHA (~2-4%). This is consistent with the research of Ridha et al.[55] where it was shown that K^+ in the 6 ring-window persists even after ion exchange. The proportion of Cs^+ in Cs-CHA is just over double that of the other cations in Ca-CHA, Ba-CHA and Sr-CHA (~9% compared to ~4%), which is expected, due to the charge difference between these cations. Zn-CHA is the chabazite zeolite possessing the smallest percentage of the extra-framework cation in the exchanged samples (~2%). This result is in good agreement with those was reported previously by Colella et al.,[63] in which the isotherm at 25 °C for the exchange of Zn into Na-chabazite was considerably lower than an upper exchange limit of 85% for Cs on Na-chabazite.

3.1. Effect of cation exchange on the morphologies of chabazite zeolites

SEM images of these exchanged chabazite zeolites (as shown in Figure 3) show that there is no significant change in the morphology with cation exchange, with the materials comprised of primary particles with sizes ranging from ~0.2-0.4 μm, which is similar previous reports for K-CHA.[55]
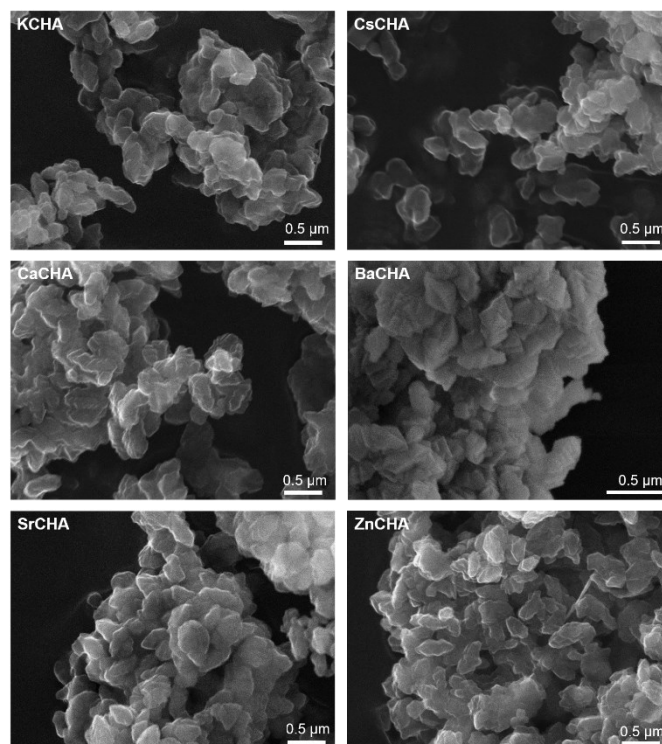

Figure 3. SEM images of ion-exchanged chabazite zeolites

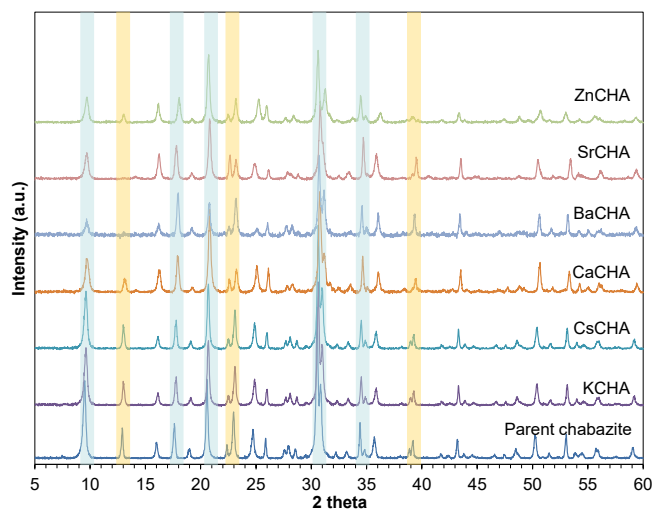### 3.2. Effect on the structural properties of chabazite zeolites

Figure 4. PXRD of parent chabazite and ion-exchanged CHA zeolites compared to simulated chabazite. Key peaks that remained the same are highlighted in light blue. Key peaks that changed or disappeared are highlighted in light orange. PXRD spectra are offset in intensity, for clarity.

In Figure 4, a full set of PXRD patterns for the ion-exchanged chabazite zeolites are presented. All peaks characteristic of the CHA framework can be seen in the PXRD pattern of K-CHA, which was expected, due to the similar EDX elemental composition of this zeolite to KNa-CHA. The main PXRD peaks at 9, 17, 21, 31 and 35 degrees 2θ in the parent chabazite zeolite appear in the powder diffraction patterns of Cs-CHA, Ca-CHA, Ba-CHA, Sr-CHA and Zn-CHA, demonstrating that the CHA framework is still maintained after ion exchange. There is little structural difference in the zeolites with divalent cations

compared to the original sample, which is evidenced by the different intensities in the peaks at 13, 22, 23 and 39 degrees 2θ. To prove that these differences are due to the appearance of extra-framework divalent cations, PXRD patterns of the chabazite zeolites were simulated using CrystalMaker and CrystalDiffract software[64] and compared with the pattern of synthesised KNa-CHA. Indeed, as shown in Figure S4 in the Supplementary data, after replacing potassium by strontium, the peak at 13 degrees 2θ almost entirely disappeared, the intensity of the peak at 22 degrees 2θ increased noticeably while the peak at 23 degrees 2θ decreased significantly and the peak at 39 degrees 2θ slightly increased in comparison to the simulated K-CHA.

In this study, SS MAS NMR (^{29}Si and ^{27}Al NMR) was employed to further investigate the effect of extra-framework cations on the structural properties of chabazite zeolites. In the chemical shifts of ^{29}Si NMR (Table S4 in SI), a very minor difference is seen between the different samples, indicating that the local environment of Si^{4+} in the framework remains unchanged. The ratio of Si/Al can be calculated using Equation 1, and results in a Si/Al ratio of ~2.0 which is consistent with the EDX results discussed above.

$$(Si/Al)_{NMR} = \frac{\sum_{n=0}^{4} I_{Si(nAl)}}{\sum_{n=0}^{4} 0.25n I_{Si(nAl)}} \qquad \textit{Equation 1}$$

where n is the number of adjacent aluminium atoms, and I is the relative integral intensity of each environment peak after deconvolution.
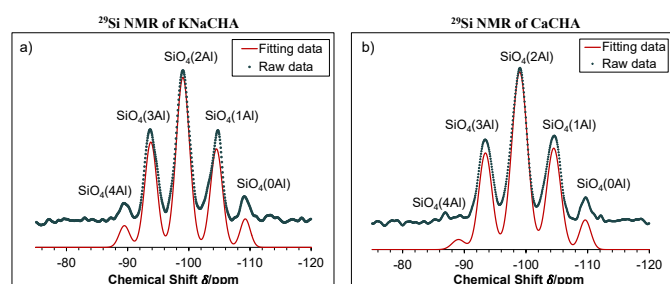

Figure 5. ^{29}Si NMR spectrum of parent KNa-CHA (a) and Ca-CHA (b). Assignment of spectra shows five distinct local environments for ^{29}Si in a zeolite.

In the ^{29}Si NMR results of KNa-CHA (Figure 5a), it can be seen that there are five high-intensity peaks in the chemical shift between -80 and -120 ppm. These peaks can be assigned to all five possible local environments of Si in the framework of the zeolite, depending on the number of aluminium atoms bonded to SiO_4,[65] hereafter referred to as $SiO_4(0Al)$, $SiO_4(1Al)$, $SiO_4(2Al)$, $SiO_4(3Al)$ and $SiO_4(4Al)$. Similar ^{29}Si NMR results are seen for all the other chabazite zeolites including K-CHA, Cs-CHA, Ca-CHA, Ba-CHA, Sr-CHA and Zn-CHA. However, in the divalent cation chabazite zeolites, the peak of $SiO_4(4Al)$ is of lower intensity than in the spectrum for the monovalent cation chabazite zeolites - see the comparison between KNa-CHA and Ca-CHA in Figure 5a and b as an example. Other ^{29}Si NMR results can be found in Figure S5 in the Supplementary data. The lowered intensity in this peak is due to the different number of aluminium atoms interacting with each cation in monovalent- and divalent chabazite.

When monovalent cations were exchanged for another species of monovalent cation during an ion exchange, almost no change to the framework average structure could be detected, for example by PXRD (see unit cell parameters in Table S2). However, when a monovalent cation, such as K^+ was exchanged for a divalent cation, for example Ca^{2+}, two K^+ atoms needed to be exchanged for one Ca^{2+} cation to retain a balanced charge on the framework (as evidenced by the EDX analysis in Table S3) and this can lead to larger displacements within the framework. Namely, exchange affects the positions of nearby tetrahedral Si and Al atoms, as the interaction between two neighbouring Al atoms is needed for each Ca^{2+} cation to change balance the structure after the exchange, leading to a contraction of the average structure to accommodate the divalent cation. This is illustrated in Figure 6, where each monovalent cation interacts with one aluminium in the zeolite framework. Thus, exchange with another monovalent cation does not affect the Si-O-Al arrangement. However, a divalent cation such as Ca^{2+} acts to charge-balance two nearby aluminium tetrahedra, as such affecting the framework and the whole crystal structure of the zeolite, reducing the distance between two aluminiums and affecting some Si-O-Al bridges which can be up to 2.4 Å in length (Si-O is 1.61 Å, and Al-O is 1.75 Å). As can be seen in the NMR results, aluminium ions in $SiO_4(4Al)$ would be affected first due to the high number of aluminium atoms corresponding to this local environment. This assumption is in a good agreement with a previous study conducted by Sartbaeva et al.[66,67]
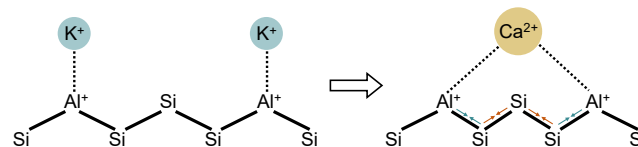

Figure 6. Proposed schematic diagram of monovalent and divalent cations interactions with aluminium atoms in the zeolite framework.
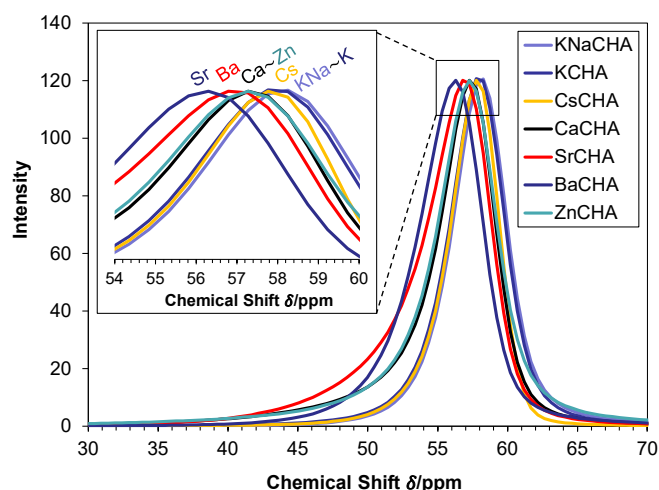

Figure 7. ^{27}Al NMR spectrum of all chabazite zeolites

^{27}Al NMR was used to provide information on the tetrahedrally-coordinated aluminium.[68] It should be recognised that it is challenging to observe features other than the tetrahedrally-coordinated aluminium in ^{27}Al NMR. Indeed, there is only one sharp peak in between 55 and 60 ppm observed in the chemical

shifts of all chabazite samples (see Figure S6 in SI). Looking closer at these results, the chemical shifts for ^{27}Al NMR of all chabazite zeolites, however, are slightly shifted. In Figure 7, the chemical shift of all cations is ordered K^+, Cs^+, $Ca^{2+} \sim Zn^{2+}$, Ba^{2+} and Sr^{2+} from right to left. The greater the valence of the cations, the stronger the interaction with aluminium in the chabazite.

3.3. Effect on the internal surface area of chabazite zeolites

To investigate the trapdoor gating ability of the different cations, BET surface area measurements of the cation exchanged chabazite zeolites were carried out using a Micromeritics 3-Flex volumetric gas sorption analysis system, using nitrogen adsorption at 77 K. Nitrogen isotherms and BET surface areas of all chabazite zeolites using N_2 at 77 K are given in Figure 8 and Table 1. Other sorption data of these samples are presented in Table S6 in the Supplementary data. Samples after gas sorption were tested again with PXRD, which confirmed that the crystallinities were preserved (see Figure S7).
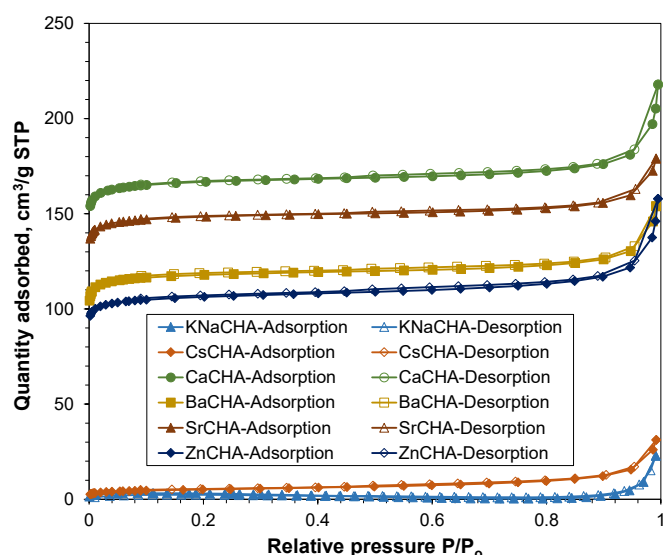

Figure 8. Nitrogen isotherms at 77 K of all chabazite zeolites

Table 1. BET results of chabazite zeolites

Samples	KNa-CHA	K-CHA	Cs-CHA	Ca-CHA	Ba-CHA	Sr-CHA	Zn-CHA
N_2 BET surface area (m² g⁻¹) at 77 K	7.6 ±0.9	7.4 ±0.6	17.4 ±0.2	529.5 ±12.0	376.0 ±8.0	471.4 ±11.0	337.1 ±8.0

Table 1 shows that the parent compound KNa-CHA has very low surface area (~8 m² g⁻¹) which is similar to the BET surface areas of K-CHA and Cs-CHA (less than 20 m² g⁻¹). However, the figures for the divalent cation chabazite zeolites including Ca-CHA, Ba-CHA, Sr-CHA and Zn-CHA were significantly higher (~340 m² g⁻¹ and above). These results are in good agreement with previously reported 77 K nitrogen sorption data for K-CHA and

Ca-CHA (20 and 649 m² g⁻¹, respectively).[55,61] As discussed in the ^{29}Si and ^{27}Al NMR results, due to the fact that each divalent cation exchanges for two monovalent cations, there are twice the number of monovalent cations in K-CHA and Cs-CHA compared to the number of divalent cations in Ca-CHA, Sr-CHA, Ba-CHA and Zn-CHA. Moreover, ionic radii are also different in these cations (see Figure 1b). The higher numbers of the large ionic radius of cations such as K^+ (δ = 1.52 Å) and Cs^+ (δ = 1.81 Å) will more effectively block the opening of the channels (d = 6.56 Å) and then prevent N_2 adsorbing into the chabazite.

4. Conclusions

In this study, a series of chabazite zeolites with monovalent and divalent extra-framework cations were synthesised successfully from zeolite Y. The results obtained from PXRD and SEM show that the synthesised samples had CHA framework structures and were nanoparticulate crystallites (size ~200-400 nm). The extra-framework cations interact differently with the aluminium in the chabazite framework depending on their valence. Ion exchanged chabazite with divalent cations showed remarkably higher nitrogen BET surface areas than those with monovalent cations. This is because the lower number of cations and the smaller size of these divalent cations at the 8 membered-ring sites would less effectively block the pore windows, allowing nitrogen to freely access the internal pores. This indicates that divalent cations would not result in good trapdoor behaviour of chabazites for selective gas storage and separation applications.

Conflicts of interest

There are no conflicts to declare.

Acknowledgements

References

1   L. Ćurković, Š. Cerjan-Stefanović and T. Filipan, *Water Res.*, 1997, **31**, 1379–1382.

2   R. P. Townsend, *Stud. Surf. Sci. Catal.*, 1991, **58**, 359–390.

3   A. Hedström, *J. Environ. Eng.*, 2001, **127**, 673–681.

4   H. W. Langmi, D. Book, A. Walton, S. R. Johnson, M. M. Al-Mamouri, J. D. Speight, P. P. Edwards, I. R. Harris and P. A. Anderson, *J. Alloys Compd.*, 2005, **404–406**, 637–642.

5   N. Kosinov, J. Gascon, F. Kapteijn and E. J. M. Hensen, *J. Memb. Sci.*, 2016, **499**, 65–79.

6   K. Kusakabe, T. Kuroda and S. Morooka, *J. Memb. Sci.*, 1998, **148**, 13–23.

7   K. S. Walton, M. B. Abney and M. D. LeVan, *Microporous Mesoporous Mater.*, 2006, **91**, 78–84.

8   Y. Hasegawa, K. Watanabe, K. Kusakabe and S. Morooka, *Sep. Purif. Technol.*, 2001, **22–23**, 319–325.

9   A. J. W. Physick, D. J. Wales, S. H. R. Owens, J. Shang, P. A. Webley, T. J. Mays and V. P. Ting, *Chem. Eng. J.*, 2016, **288**, 161–168.

10 K. Sahner, G. Hagen, D. Schönauer, S. Reiß and R. Moos, *Solid State Ionics*, 2008, **179**, 2416–2423.

11 D. P. Mann, K. F. E. Pratt, T. Paraskeva, I. P. Parkin and D. E. Williams, *IEEE Sens. J.*, 2007, **7**, 551–556.

12 X. Xu, J. Wang and Y. Long, *Sensors*, 2006, **6**, 1751–1764.

13 H. Bordeneuve, D. J. Wales, A. J. W. Physick, H. V. Doan, V. P. Ting and C. R. Bowen, *Microporous Mesoporous Mater.*, 2018, **260**, 208–216.

14 M. Iwamoto, H. Furukawa, Y. Mine, F. Uemura, S. I. Mikuriya and S. Kagawa, *J. Chem. Soc. - Ser. Chem. Commun.*, 1986, **0**, 1272–1273.

15 M. Iwamoto, H. Yahiro, S. Shundo, Y. Yu-u and N. Mizuno, *Appl. Catal.*, 1991, **69**, L15–L19.

16 M. Iwamoto, H. Yahiro, Y. Mine and S. Kagawa, *Chem. Lett.*, 1989, **18**, 213–216.

17 B. M. Weckhuysen, D. Wang, M. P. Rosynek and J. H. Lunsford, *J. Catal.*, 1998, **175**, 338–346.

18 C. Baerlocher, Database of Zeolite Structures, http://www.iza-structure.org/databases/, (accessed 3 September 2019).

19 M. Choi, K. Na, J. Kim, Y. Sakamoto, O. Terasaki and R. Ryoo, *Nature*, 2009, **461**, 246–249.

20 H. Wang and T. J. Pinnavaia, *Angew. Chemie - Int. Ed.*, 2006, **45**, 7603–7606.

21 L. Li, J. Dong, T. M. Nenoff and R. Lee, *J. Memb. Sci.*, 2004, **243**, 401–404.

22 K. Na, M. Chol, W. Park, Y. Sakamoto, O. Terasakl and R. Ryoo, *J. Am. Chem. Soc.*, 2010, **132**, 4169–4177.

23 A. Inayat, I. Knoke, E. Spiecker and W. Schwieger, *Angew. Chemie - Int. Ed.*, 2012, **51**, 1962–1965.

24 L. Martins, R. T. Boldo and D. Cardoso, *Microporous Mesoporous Mater.*, 2007, **98**, 166–173.

25 Y. Kuwahara, J. Aoyama, K. Miyakubo, T. Eguchi, T. Kamegawa, K. Mori and H. Yamashita, *J. Catal.*, 2012, **285**, 223–234.

26 Y. Li, J. Liu and W. Yang, *J. Memb. Sci.*, 2006, **281**, 646–657.

27 M. B. Park, Y. Lee, A. Zheng, F. S. Xiao, C. P. Nicholas, G. J. Lewis and S. B. Hong, *J. Am. Chem. Soc.*, 2013, **135**, 2248–2255.

28 B. Z. Zhan and E. Iglesia, *Angew. Chemie - Int. Ed.*, 2007, **46**, 3697–3700.

29 M. L. U. Cornelius, L. Price, S. A. Wells, L. F. Petrik and A. Sartbaeva, *Zeitschrift fur Krist. - Cryst. Mater.*, 2019, **234**, 461–468.

30 L. Regli, A. Zecchina, J. G. Vitillo, D. Cocina, G. Spoto, C. Lamberti, K. P. Lillerud, U. Olsbye and S. Bordiga, *Phys. Chem. Chem. Phys.*, 2005, **7**, 3197–3203.

31 A. Zecchina, S. Bordiga, J. G. Vitillo, G. Ricchiardi, C. Lamberti, G. Spoto, M. Bjørgen and K. P. Lillerud, *J. Am. Chem. Soc.*, 2005, **127**, 6361–6366.

32 S. M. Robinson, W. D. Arnold and C. H. Byers, 1991, pp. 133–152.

33 N. T. T. Nguyen, H. Furukawa, F. Gándara, H. T. Nguyen, K. E. Cordova and O. M. Yaghi, *Angew. Chemie - Int. Ed.*, 2014, **53**, 10645–10648.

34 M. Moliner, J. E. Gabay, C. E. Kliewer, R. T. Carr, J. Guzman, G. L. Casty, P. Serna and A. Corma, *J. Am. Chem. Soc.*, 2016, **138**, 15743–15750.

35 F. N. Ridha and P. A. Webley, *Sep. Purif. Technol.*, 2009, **67**, 336–343.

36 A. Nearchou, P. R. Raithby and A. Sartbaeva, *Microporous Mesoporous Mater.*, 2018, **255**, 261–270.

37 A. Nearchou, M. L. U. Cornelius, J. M. Skelton, Z. L. Jones, A. B. Cairns, I. E. Collings, P. R. Raithby, S. A. Wells and A. Sartbaeva, *Molecules*, 2019, **24**, 641.

38 Y. Zhou, W. Chen, P. Wang and Y. Zhang, *Microporous Mesoporous Mater.*, 2018, **271**, 273–283.

39 B. Dong, S. Belkhair, M. Zaarour, L. Fisher, J. Verran, L. Tosheva, R. Retoux, J. P. Gilson and S. Mintova, *Nanoscale*, 2014, **6**, 10859–10864.

40 M. Moliner, F. Rey and A. Corma, *Angew. Chemie - Int. Ed.*, 2013, **52**, 13880–13889.

41 A. Sartbaeva, S. A. Wells, M. M. J. Treacy and M. F. Thorpe, *Nat. Mater.*, 2006, **5**, 962–965.

42 H. Awala, J. P. Gilson, R. Retoux, P. Boullay, J. M. Goupil, V. Valtchev and S. Mintova, *Nat. Mater.*, 2015, **14**, 447–451.

43 V. Valtchev and S. Mintova, *Microporous Mesoporous Mater.*, 2001, **43**, 41–49.

44 H. V. Doan, H. Amer Hamzah, P. Karikkethu Prabhakaran, C. Petrillo and V. P. Ting, *Nano-Micro Lett.*, 2019, **11**, 54.

45 H. V. Doan, F. Cheng, T. Dyirakumunda, M. R. J. Elsegood, J. Chin, O. Rowe, C. Redshaw and V. P. Ting, *Crystals*, 2020, **10**, 17.

46 S. Xu, A. Zheng, Y. Wei, J. Chen, J. Li, Y. Chu, M. Zhang, Q. Wang, Y. Zhou, J. Wang, F. Deng and Z. Liu, *Angew. Chemie - Int. Ed.*, 2013, **52**, 11564–11568.

47 F. Bleken, M. Bjørgen, L. Palumbo, S. Bordiga, S. Svelle, K. P. Lillerud and U. Olsbye, *Top. Catal.*, 2009, **52**, 218–228.

48 J. Wang, H. Zhao, G. Haller and Y. Li, *Appl. Catal. B Environ.*, 2017, **202**, 346–354.

49 U. De-La-Torre, B. Pereda-Ayo, M. Moliner, J. R. González-Velasco and A. Corma, *Appl. Catal. B Environ.*, 2016, **187**, 419–427.

50 T. De Baerdemaeker and D. De Vos, *Nat. Chem.*, 2013, **5**, 89–90.

51 E. García-Pérez, J. B. Parra, C. O. Ania, A. García-Sánchez, J. M. Van Baten, R. Krishna, D. Dubbeldam and S. Calero, *Adsorption*, 2007, **13**, 469–476.

52 J. Zhang, R. Singh and P. A. Webley, *Microporous Mesoporous Mater.*, 2008, **111**, 478–487.

53 J. Shang, G. Li, R. Singh, P. Xiao, J. Z. Liu and P. A. Webley, *J. Phys. Chem. C*, 2013, **117**, 12841–12847.

54 J. Shang, G. Li, R. Singh, Q. Gu, K. M. Nairn, T. J. Bastow, N. Medhekar, C. M. Doherty, A. J. Hill, J. Z. Liu and P. A. Webley, *J. Am. Chem. Soc.*, 2012, **134**, 19246–19253.

55 F. N. Ridha, Y. Yang and P. A. Webley, *Microporous Mesoporous Mater.*, 2009, **117**, 497–507.

56 A. Alberti, E. Galli, G. Vezzalini, E. Passaglia and P. F. Zanazzi, *Zeolites*, 1982, **2**, 303–309.

57 P. Ugliengo, C. Busco, B. Civalleri and C. M. Zicovich-Wilson,

Mol. Phys., 2005, **103**, 2559–2571.

58 D. T. Bostick, W. D. Arnold, B. Guo and M. W. Burgess, *Sep. Sci. Technol.*, 1997, **32**, 793–811.

59 L. J. Smith, H. Eckert and A. K. Cheetham, *J. Am. Chem. Soc.*, 2000, **122**, 1700–1708.

60 J. Emsley, *Found. Chem.*, 2020, **22**, 275–277.

61 J. Shang, G. Li, R. Singh, P. Xiao, J. Z. Liu and P. A. Webley, *J. Phys. Chem. C*, 2010, **114**, 22025–22031.

62 M. Calligaris, G. Nardin and L. Randaccio, *Zeolites*, 1983, **3**, 205–208.

63 C. Colella, M. De' Gennaro, A. Langella and M. Pansini, *Sep. Sci. Technol.*, 1998, **33**, 467–481.

64 D. C. Palmer, *Zeitschrift fur Krist. - Cryst. Mater.*, 2015, **230**, 559–572.

65 M. T. Melchior, D. E. W. Vaughan and C. F. Pictroski, *J. Phys. Chem.*, 1995, **99**, 6128–6144.

66 A. Sartbaeva, N. H. Rees, P. P. Edwards, A. J. Ramirez-Cuesta and E. Barney, *J. Mater. Chem. A*, 2013, **1**, 7415–7421.

67 L. Price, K. Leung and A. Sartbaeva, *Magnetochemistry*, 2017, **3**, 42.

68 B. Boddenberg, High-resolution solid-state NMR of silicates and zeolites, https://www.osti.gov/biblio/6743230, (accessed 28 November 2020).

69 L. Lutterotti, M. Bortolotti, G. Ischia, I. Lonardelli and H.-R. Wenk, in *Tenth European Powder Diffraction Conference*, OLDENBOURG WISSENSCHAFTSVERLAG, 2015.

Supplementary data

Effect of mono- and divalent extra-framework cations on the structure and accessibility of porosity in chabazite zeolites

Huan V. Doan,[*a,b] Ka Ming Leung,[c] Valeska P. Ting[*d] and Asel Sartbaeva[*e]

[a.]*School of Chemistry, University of Bristol, Bristol BS8 1TS, UK.*

[b.] *Department of Oil Refining and Petrochemistry, Hanoi University of Mining and Geology, Duc Thang, Bac Tu Liem, Hanoi, Vietnam.*

[c.]*Department of Chemistry, The University of Hong Kong, Pokfulam, Hong Kong SAR, China.*

[d.]*Department of Mechanical Engineering, University of Bristol, Bristol BS8 1TR, UK.*

[e.]*Department of Chemistry, University of Bath, Bath BA2 7AY, UK.*

Corresponding authors. Email: huan.doan@bristol.ac.uk (HVD); v.ting@bristol.ac.uk (VPT) and a.sartbaeva@bath.ac.uk (AS)

Contents

1. Characterisation techniques

1.1. Scanning electron microscopy and energy-dispersive X-ray spectroscopy

Low resolution micrographs were taken using a JEOL SEM6480LV scanning electron microscope (SEM) with back scattering electrons (BSE). Energy-dispersive X-ray spectroscopy (EDX) data were acquired using an Oxford INCA X-ray analyser attached to the microscope. High resolution micrographs were taken using the JEOL FESEM6301F field emission scanning electron microscope at the University of Bath. Source: cold cathode UHV field emission conical anode gun, accelerating voltage: 5 - 20 kV, magnification from 10.000 times to 40.000 times.

1.2. Powder X-ray diffraction

Room temperature Powder X-ray diffraction (PXRD) results below were obtained using a BRUKER AXS D8-Advance with Vantec-1 detector using Cu Kα (λ = 1.5418 Å) as the source of X-ray radiation, in flat plate geometry with a spinner speed is 15 rpm, at the Department of Chemistry, University of Bath.

1.3. Simulation using CrystalMaker and CrystalDiffract

Crystal structures of chabazite zeolites were simulated in CrystalMaker for Windows (Version 9.1.4 (633), licensed to the University of Bath: Serial number: 2930) according to the data of Calligaris *et al.,*[62] space group is r$\bar{3}$m *a* = *b* = *c* = 9.459Å; α = β = γ = 94.07°. The atomic positions used are given in Table S1. The powder diffraction patterns of simulated samples were then compared with that of synthesised ones in CrystalDiffract for Window version 6.5.0 (211) licensed to University of Bath (serial number: 1166) to confirm the presence of cations in chabazite zeolites.

Table S1. Atomic positions used for simulation of chabazite structure

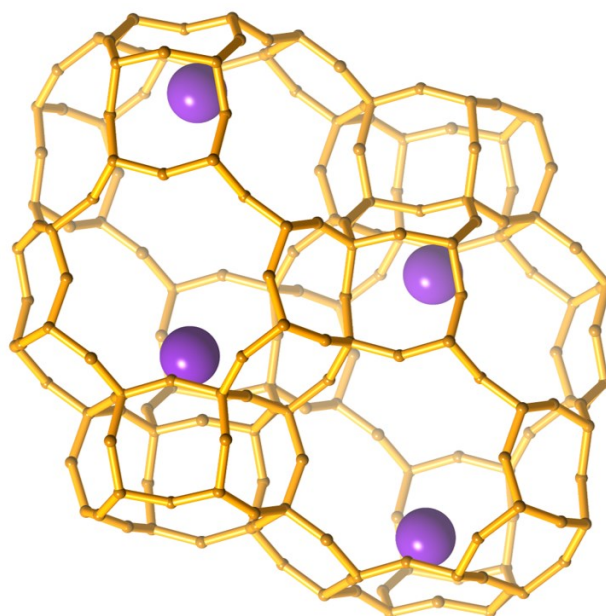| Label	Site Occupancy	x	y	z
Si	Si 0.67 Al 0.33	0.1033	0.3331	0.8743
O1	O 1.00	0.2665	-0.2665	0.0000
O2	O 1.00	0.1506	-0.1506	0.5000
O3	O 1.00	0.2503	0.2503	0.8930
O4	O 1.00	0.0204	0.0204	0.3193
K1	K 0.97	0.2222	0.2222	0.2222
K2	K 0.15	0.5611	0.5611	0.2506
K3	K 0.22	0.5255	0.5255	0.1064

Figure S1. Crystal structure of K-CHA. Potassium atoms are presented by purple balls. Images generated using CrystalMaker®: a crystal and molecular structures program for Windows. CrystalMaker Software Ltd, Oxford, England

1.4. Cell parameters analysis

Le Bail analysis was performed on the diffraction spectra to calculate the cell parameters of synthesised chabazite samples. In each analysis, PXRD data (.xy file) and CHA structure (as shown in Table S1) were loaded in MAUD program[69] using the following setting, angular calibration: instrument misalignment, geometry: Bragg-Brentano, instrument broadening:

Caglioti PV, Size-Strain model: Anisotropic. Each structure was refined until the weighted profile R-factor (R_{wp}) value was below 18. An example of a refined XRD structure is given in Figure S2.
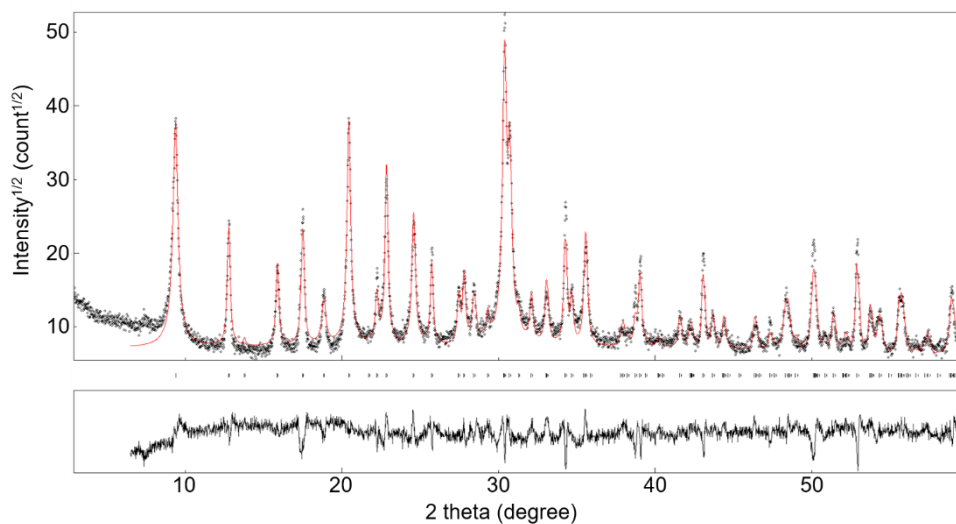

Figure S2: Refined PXRD patterns of KNaCHA

1.5. Solid state magic angle spinning nuclear magnetic resonance

^{29}Si and ^{27}Al NMR spectrum of chabazite zeolites were measured using a VARIAN VNMRS 400 spectrometer using direct excitation (DE) method, with tetramethylsilane and 1M aqueous aluminium nitrate solution as references. The spinning rate of ^{29}Si NMR was 6.8 kHz, ^{27}Al NMR was 14 kHz. Solid state NMR spectra were obtained at the EPSRC UK National Solid-state NMR service at Durham University. The data then were fitted using Solver program in Excel to a Pseudo-Gaussian function.

1.6. Gas sorption

The surface area of all chabazite zeolites in this research were determined on samples of ~100 mg using nitrogen sorption at 77 K with a Micromeritics 3-Flex volumetric gas sorption analysis system. Nitrogen was purchased from Air Products with purity of 99.9999%. Samples were degassed at 350 °C under dynamic high (10^{-6} mbar) vacuum for 12 h prior to analysis.

2. Additional information and results

2.1. Cell parameters

Table S2. Cell parameters of synthesised chabazite zeolites

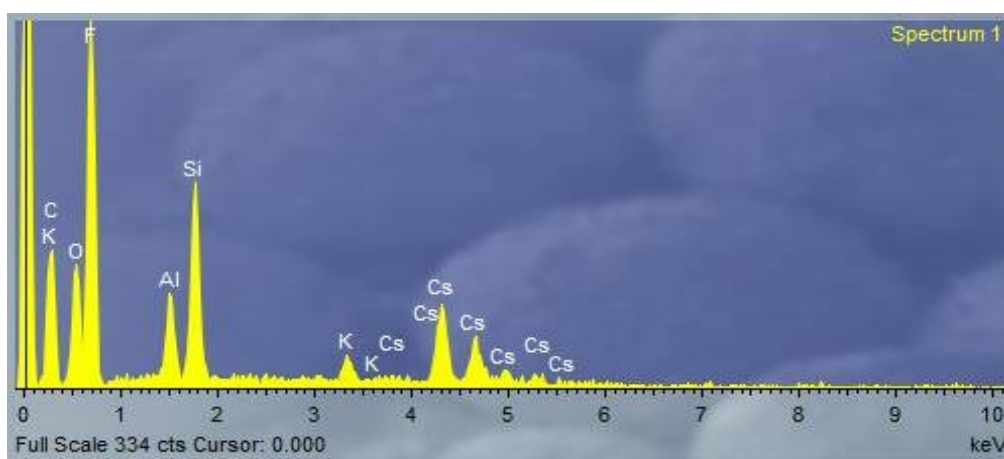| Rhombohedral setting (r$\bar{3}$m)	KNA-CHA	Cs-CHA	Ca-CHA	Ba-CHA	Sr-CHA	Zn-CHA
a (Angstrom)	9.461	9.463	9.437	9.449	9.438	9.445
alpha (degree)	94.029	94.217	94.202	94.270	93.863	94.676

2.2. Energy-dispersive X-ray spectroscopy

Figure S3. EDX spectrum of Cs-CHA

Table S3. The elemental composition of synthesised chabazite zeolites (atomic%)

Samples	O	Na	Al	Si	K	Cs	Ca	Sr	Ba	Zn
KNa-CHA	61.81 ±4.00	0.10 ±0.12	8.63 ±0.60	18.99 ±1.60	10.46 ±2.60	-	-	-	-	-
K-CHA	65.38 ±4.04	-	8.15 ±0.70	18.23 ±1.98	8.24 ±1.40	-	-	-	-	-
Cs-CHA	56.83 ±7.98	-	9.19 ±0.70	21.93 ±2.08	2.70 ±1.16	9.36 ±4.76	-	-	-	-
Ca-CHA	69.08 ±3.14	-	8.08 ±0.8	17.62 ±2.05	2.30 ±0.43	-	2.93 ±0.32	-	-	-
Sr-CHA	65.79 ±3.44	-	8.95 ±0.83	19.69 ±2.01	2.31 ±0.31	-	-	3.26 ±0.42	-	-
Ba-CHA	64.94 ±2.29	-	9.03 ±0.39	19.68 ±1.04	2.38 ±0.56	-	-	-	3.96 ±0.61	-
Zn-CHA	66.94 ±5.55	-	8.39 ±0.87	18.37 ±2.56	4.03 ±1.23	-	-	-	-	2.26 ±0.91

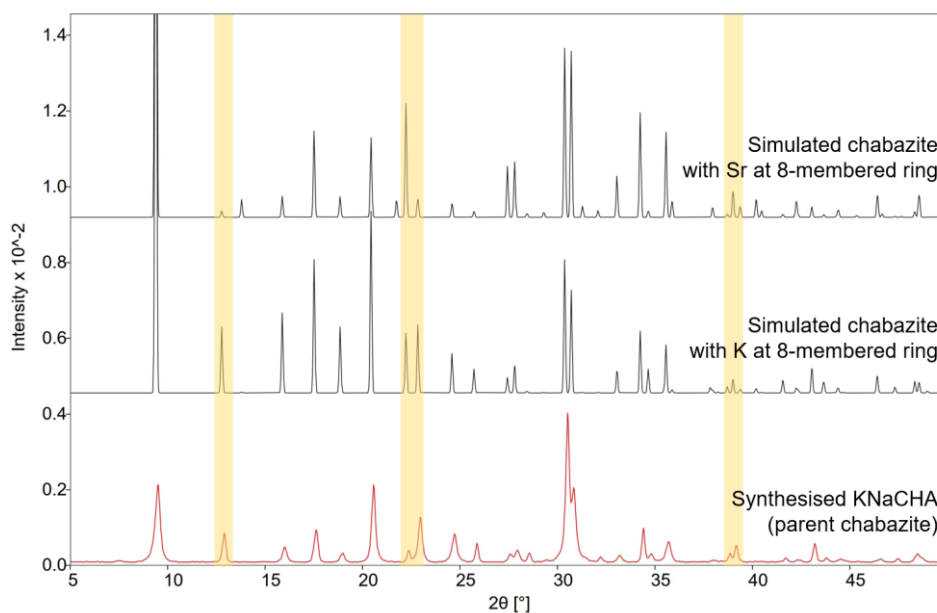## 2.3. Simulation using CrystalMaker and CrystalDiffract

Figure S4. PXRD patterns of simulated K-CHA and simulated Sr-CHA (K and Sr positioned at the eight-membered ring) in comparison to PXRD pattern of synthesised KNa-CHA.

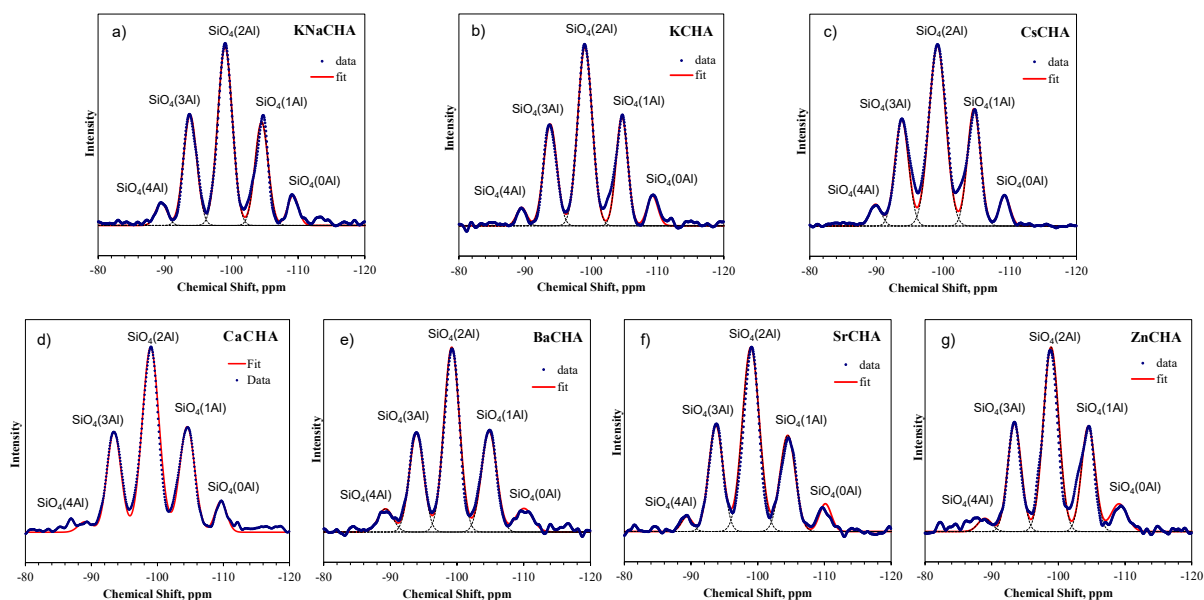## 2.4. Solid-state magic-angle spinning nuclear magnetic resonance

^{29}Si NMR:

Figure S5. ^{29}Si NMR results of all chabazite zeolites

KNa-CHA: ^{29}Si NMR (79 MHz, none) δ ppm -108.85 (br. s., 2 Si) -104.63 (br. s., 10 Si) -98.93 (br. s., 19 Si) -93.48 (br. s., 11 Si) -89.26 (br. s., 2 Si). K-CHA: ^{29}Si NMR (79 MHz, none) δ ppm -109.10 (br. s., 3 Si) -104.63 (br. s., 23 Si) -98.68 (br. s., 47 Si) -93.48 (br. s., 25 Si) -89.51 (br. s., 4 Si). Cs-CHA: ^{29}Si NMR (79 MHz, none) δ ppm -108.85 (br. s., 7 Si) -104.39 (br. s., 28 Si) -98.68 (br. s., 42 Si) -93.48 (br. s., 18 Si) -89.26 (br. s., 3 Si). Ca-CHA: ^{29}Si NMR (79 MHz, none) δ ppm -109.59 (br. s., 2 Si) -104.39 (br. s., 22 Si) -98.68 (br. s., 49 Si) -93.23 (br. s., 26 Si) -89.26 (br. s., 3 Si). Ba-CHA: ^{29}Si NMR (79 MHz, none) δ ppm -109.59 (br. s., 3 Si) -104.63 (br. s., 24 Si) -99.18 (br. s., 46 Si) -93.72 (br. s., 27 Si) -88.52 (br. s., 2 Si). Sr-CHA: ^{29}Si NMR (79 MHz, none) δ ppm -109.59 (br. s., 2 Si) -104.39 (br. s., 21 Si) -98.93 (br. s., 47 Si) -93.48 (br. s., 28 Si) -89.01 (br. s., 3 Si). Zn-CHA: ^{29}Si NMR (79 MHz, none) δ ppm -109.35 (br. s., 4 Si) -104.39 (br. s., 25 Si) -98.68 (br. s., 46 Si) -93.23 (br. s., 25 Si) -89.73 - -85.33 (m, 2 Si).

Table S4. The chemical shifts from ^{29}Si and calculated Si/Al ratios of chabazite zeolites

Samples	SiO$_4$(0Al)	SiO$_4$(1Al)	SiO$_4$(2Al)	SiO$_4$(3Al)	SiO$_4$(4Al)	Si/Al
KNa-CHA	-109.2	-104.5	-99.0	-93.8	-89.5	2.00
K-CHA	-109.4	-104.5	-99.0	-93.8	-89.5	2.00
Cs-CHA	-109.2	-104.6	-99.2	-94.0	-89.8	2.04
Ca-CHA	-109.7	-104.4	-98.9	-93.5	-87.9	2.10
Ba-CHA	-110.1	-104.8	-99.2	-93.9	-89.3	2.06
Sr-CHA	-109.8	-104.6	-99.0	-93.8	-89.2	2.04
Zn-CHA	-109.4	-104.2	-98.8	-93.4	-87.9	2.08

^{27}Al NMR:
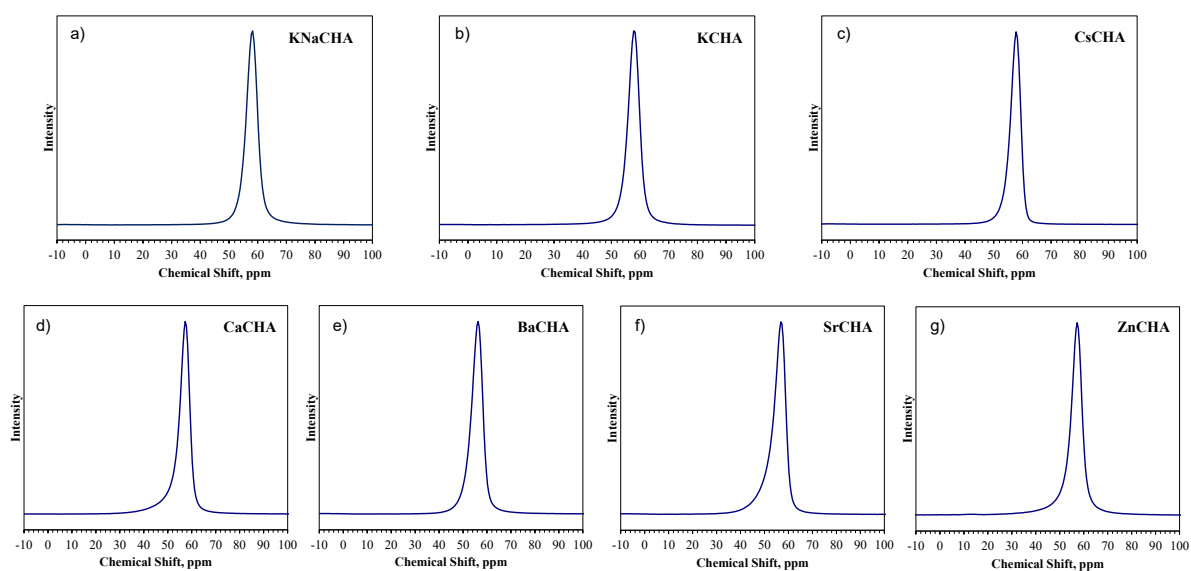
Figure S6. ^{27}Al NMR results of all chabazite zeolites

KNA-CHA: ^{27}Al NMR (104 MHz, none) δ ppm 58.29 (br. s., 160 Al). K-CHA: ^{27}Al NMR (104 MHz, none) δ ppm 57.80 (br. s., 69 Al). Cs-CHA: ^{27}Al NMR (104 MHz, none) δ ppm 57.80 (br. s., 98 Al). Ca-CHA: ^{27}Al NMR (104 MHz, none) δ ppm 57.31 (br. s., 97 Al). Ba-CHA: ^{27}Al NMR (104 MHz, none) δ ppm 56.33 (br. s., 98 Al). Sr-CHA: ^{27}Al NMR (104 MHz, none) δ ppm 56.82 (br. s., 98 Al). Zn-CHA: ^{27}Al NMR (104 MHz, none) δ ppm 57.31 (br. s., 100 Al).

Table S5. Chemical shifts from ^{27}Al of chabazite zeolites

Samples	KNa-CHA	K-CHA	Cs-CHA	Ca-CHA	Ba-CHA	Sr-CHA	Zn-CHA
Chemical shifts, ppm	58.26	58.26	57.77	57.28	56.30	56.79	57.28

2.5. Gas sorption

Table S6. Nitrogen sorption data of all chabazite zeolites

Samples	BET surface area (m² g⁻¹)	Langmuir surface area (m² g⁻¹)	t-plot micropore area (m² g⁻¹)	BJH desorption pore volume (cm³ g⁻¹)
KNa-CHA	7.6	13.9	13.7	0.024
Cs-CHA	17.4	58.3	4.6	0.044
Ca-CHA	529.5	780.0	494.3	0.067
Ba-CHA	376.0	574.3	345.0	0.061
Sr-CHA	471.4	698.7	441.3	0.054
Zn-CHA	337.1	535.1	305.0	0.087

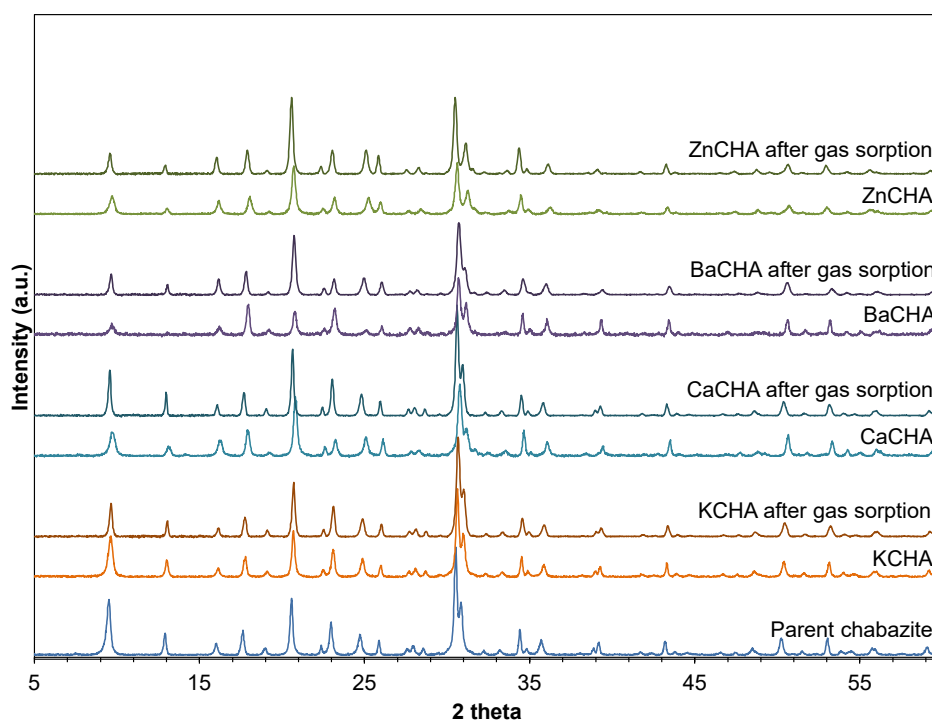## *2.6. Powder X-ray diffraction of exchanged chabazite zeolites after gas sorption*

Figure S7. PXRD results of exchanged chabazite zeolites after gas sorption